Available online at www.sciencedirect.com
ScienceDirect
Journal of Power Sources 179 (2008) 497–503
JOURNAL OF POWER SOURCES
www.elsevier.com/locate/jpowsour

Temperature and humidity dependence of the electrode polarization in intermediate-temperature fuel cells employing CsH_2PO_4/SiP_2O_7-based composite electrolytes

Shuichi Yoshimi, Toshiaki Matsui *, Ryuji Kikuchi, Koichi Eguchi

Department of Energy and Hydrocarbon Chemistry, Graduate School of Engineering, Kyoto University, Nishikyo-ku, Kyoto 615-8510, Japan

Received 19 November 2007; received in revised form 26 December 2007; accepted 4 January 2008
Available online 11 January 2008

Abstract

The polarization behaviors of platinum electrode were investigated with a single cell employing CsH_2PO_4/SiP_2O_7-based composite electrolyte. The electrochemical measurements were conducted in the temperature range of 180–240 °C under various humidity conditions. The cell performance was enhanced during several discharge cycles, and then the steady state was attained. The active triple phase boundary (TPB) appears to be spontaneously formed. The polarization behaviors for both anode and cathode were strongly affected by the electrolyte conductivity due to its humidity dependence. In accordance with this tendency, the maximum performance was achieved at 220 °C in 30% humidified condition whereas the deterioration was observed at 240 °C. Throughout the analysis, however, the performance limitation was mainly due to cathodic polarization at every condition. The cathodic overpotential showed a linear dependence against the log of current density at each temperature, which can be expressed as a Tafel equation. Then, the influence of steam concentration and temperature on the electrochemical kinetics was also discussed.

Keywords: Intermediate-temperature fuel cells; Electrode polarization; Oxioacid-based electrolyte; CsH_2PO_4/SiP_2O_7-based composite

1. Introduction

Fuel cells are attractive alternatives to traditional power sources because they can directly convert chemical energy into electrical energy with low emissions and high efficiency. Cell types are classified based on electrolyte materials. Polymer electrolyte fuel cell (PEFC) is one of the promising systems for both stationary and transportation applications. Hydrated perfluorosulfonic acid membranes such as Nafion® are widely used as electrolytes, which limit the operating temperature below 100 °C resulting in critical issues such as CO poisoning of Pt electrodes [1–3], complicated fuel processing and water management. Heat-resistive electrolytes operative in the temperature range up to 300 °C will readily overcome these problems, and many studies have been extensively conducted for the development of intermediate-temperature fuel cells (<300 °C) [4–15].

We have recently developed a new proton-conductive solid-state electrolyte based on CsH_2PO_4/SiP_2O_7 composite [16]. This composite exhibited high proton conductivity of 44 mS cm^{-1} at 266 °C under 30% H_2O/Ar atmosphere. The operation of the fuel cell using this electrolyte was demonstrated successfully at 220 °C. In this composite, ionic-conduction phase of $CsH_5(PO_4)_2$ is responsible for high conductivity, which is formed via chemical reaction between CsH_2PO_4 and SiP_2O_7 matrix during initial heat-treatment at intermediate temperatures [16,17]. Good compatibility between $CsH_5(PO_4)_2$ and SiP_2O_7 has been also confirmed [18]. It is noted that the composite is stable in the solid-state at elevated temperatures despite the melting of $CsH_5(PO_4)_2$ component above 150 °C. This may be due to the interfacial interaction between the conduction phase and matrix. Several groups have also reported fuel cells employing a series of oxoacid-based electrolytes such as CsH_2PO_4 and $CsHSO_4$ above 150 °C [4–6]. In these types of fuel cells, generally, the

* Corresponding author. Tel.: +81 75 383 2523; fax: +81 75 383 2520.
E-mail address: matsui@elech.kuic.kyoto-u.ac.jp (T. Matsui).

0378-7753/$ – see front matter © 2008 Elsevier B.V. All rights reserved.
doi:10.1016/j.jpowsour.2008.01.003

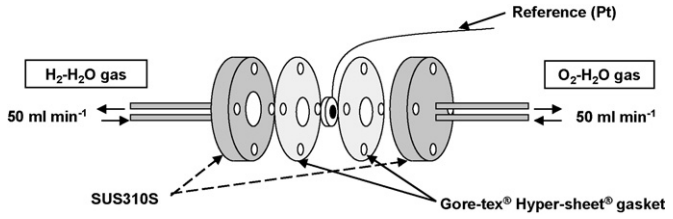

Fig. 1. Schematic illustration of a single cell.

electrochemical reaction occurs at the triple phase boundary (TPB) of gas/solid electrode/solid electrolyte interface. In fact, however, proton-conductive oxoacid-based electrolytes will be in a highly viscous molten state rather than in a solid state at the operating temperature to achieve high ionic conductivity, which is different from that in the case of phosphoric acid fuel cell (PAFC). Therefore, the structure of TPB has to be optimized. Addition of ion-conductive materials in the electrode is one of the effective methods to expand the TPB, as can be seen in PEFC and solid oxide fuel cell [19,20]. However, there are few reports on electrode activity and kinetics in the temperature range of 200–300 °C by using oxoacid-based electrolytes. In this study, the polarization behaviors of platinum electrode for both in anode and cathode were investigated in order to obtain the design guide with a single cell employing CsH_2PO_4/SiP_2O_7-based composite electrolyte at intermediate temperatures.

2. Experimental

Cesium dihydrogen phosphate, CsH_2PO_4 (CDP), was synthesized from H_3PO_4 (Wako Pure Chemical Industries Ltd.) and Cs_2CO_3 (Sigma–Aldrich Inc.). Pyrophosphate of SiP_2O_7 was synthesized from H_3PO_4 and SiO_2 (NIPPON Silica. Ltd.) as starting materials [17]. The resulting powders were mixed to be the composite electrolyte of CsH_2PO_4/SiP_2O_7 in the molar ratio of 1/2. Composite powder was uniaxially pressed with Pt/C carbon paper (E-TEK Inc., Pt loadings: 1 mg cm^{-2}) to form the membrane electrolyte assembly (MEA, diameter: 13 mm, thickness: *ca.* 1.3 mm, electrode area: 0.283 cm^2), and then the resulting MEA was heat-treated at 220 °C for 1 h.

Fig. 1 shows the cell configuration used for power generation and polarization measurements. A reference electrode was made with platinum wire on the anode-side surface of electrolyte, and platinum mesh was used as a current collector. Hydrogen and oxygen were fed to anode and cathode, respectively. Water concentration in the feeding gas was controlled in the range of 0–30% by changing the bubbling temperature. In the case of 0% H_2O, unhumidified fuel or oxidant was supplied directly to the experimental apparatus. Total flow of gaseous mixture was fixed so as to be 50 ml min^{-1}. Electrode polarization resistance was measured using ac impedance spectroscopy at atmospheric pressure in the temperature range of 180–240 °C (Solartron 1260 frequency-response analyzer and Solartron 1287 potentiostat). The applied frequency was in the range of 0.01 Hz to 1 MHz. Current-interruption method was also used to analyze electrode overpotential (Hokuto Denko HC-111).

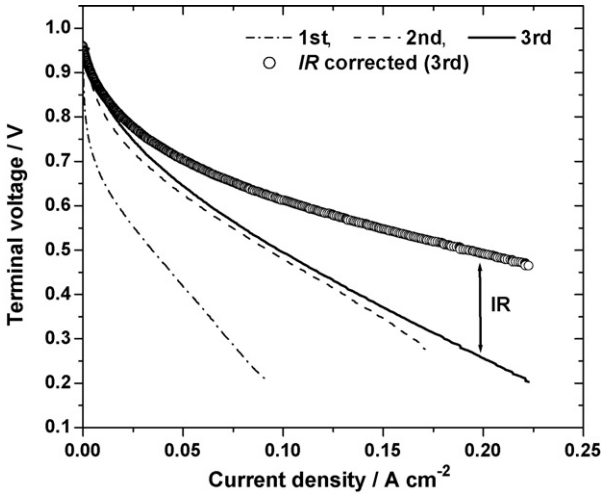

Fig. 2. *I–V* curve for a single cell at 200 °C (30% H_2O/H_2, Pt/C|CsH_2PO_4/SiP_2O_7|Pt/C, 30% H_2O/O_2).

3. Results and discussion

3.1. Polarization behavior

Typical *I–V* characteristics at intermediate temperatures are shown in Fig. 2. The performance improved drastically during three consecutive measurements, and then the steady state was attained. In the first discharge, the steep drop in a terminal voltage at low current density region was observed. This indicates the extremely low electrocatalytic activity due to the insufficient electrode/electrolyte interface formation. As mentioned above, the composite electrolyte of CsH_2PO_4/SiP_2O_7 forms the new conduction phase of $CsH_5(PO_4)_2$ in the initial heat-treatment at 220 °C. The resulting salt melts above 150 °C and is in a molten state in the composite [16]. Thus, the molten salt in the vicinity of the interface should penetrate into Pt/C electrode during subsequent measurements, resulting in the formation of active TPB. The open circuit voltage (OCV) was stable and *ca.* 100–200 mV lower than theoretical values at every temperature, which was comparable to that for phosphoric acid fuel cells. This can be explained by the formation of oxides on the Pt surface at high potential [21]. Carbon oxidation may also lead to low OCV at intermediate temperatures [22]. In the previous paper, we reported the OCV of 0.78 V at 220 °C by using the same cell configuration due to a low relative density of electrolyte [17]. Thus, we can guess that the employed electrolyte is sufficiently dense and the obtained OCVs are higher limits. The plot of open circle is correspondent to the *IR*-corrected curve of the third measurement. Even at high current density region, the performance limitation was mainly due to the electrode polarization. The optimization of electrocatalysts is required for the development of intermediate-temperature fuel cells. Then, the electrode polarization was analyzed by ac impedance spectroscopy.

Impedance spectra of a single cell with two-electrode system measured at various terminal voltages are shown in Fig. 3. The impedance spectra included the polarization resistance of both electrodes and appeared to consist of two arcs at high- and low-

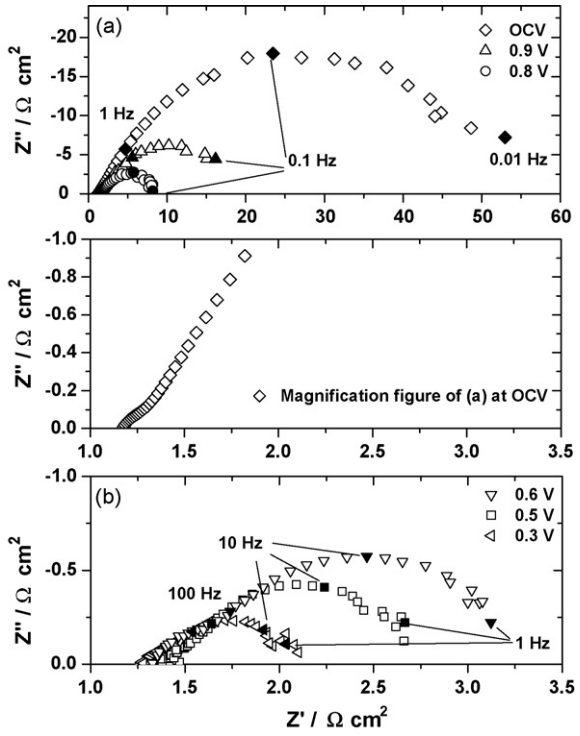

Fig. 3. Impedance spectra of a single cell at various terminal voltage at 200 °C (30% H_2O/H_2, Pt/C|CsH_2PO_4/SiP_2O_7|Pt/C, 30% H_2O/O_2): (a) OCV–0.8 V; (b) 0.6–0.3 V.

frequencies. The arc at low-frequencies dramatically decreased with passing current, whereas the other one at high-frequencies was less sensitive to the terminal voltage. This means that at least two processes are involved. Corresponding impedance spectra of anode and cathode are shown in Figs. 4 and 5, respectively, which were measured using a three-electrode cell. In anode, the polarization resistance was almost independent of the electrode potential with a value of *ca.* 0.3 Ωcm^2, indicating that the hydrogen oxidation is sufficiently fast. On the other hand, the polarization resistance in cathode was extremely large under the open circuit condition and continuously decreased with increasing current. As can be seen in Fig. 2, this resulted in low performance at low current density region during discharge operation. Judging from the frequency-response in each electrode, high- and low-frequency arcs observed in two-electrodes system can be roughly assigned to anode and cathode reactions, respectively. At this stage, however, the equivalent circuit

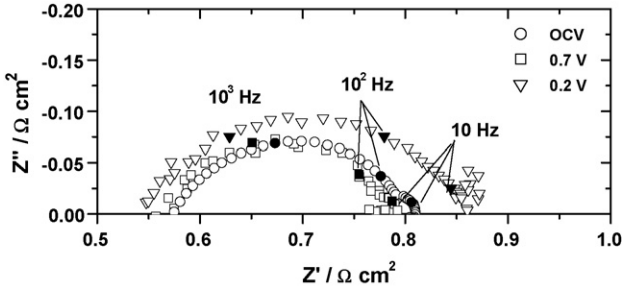

Fig. 4. Impedance spectra of anode in the third measurement of *I–V* curve in Fig. 2.

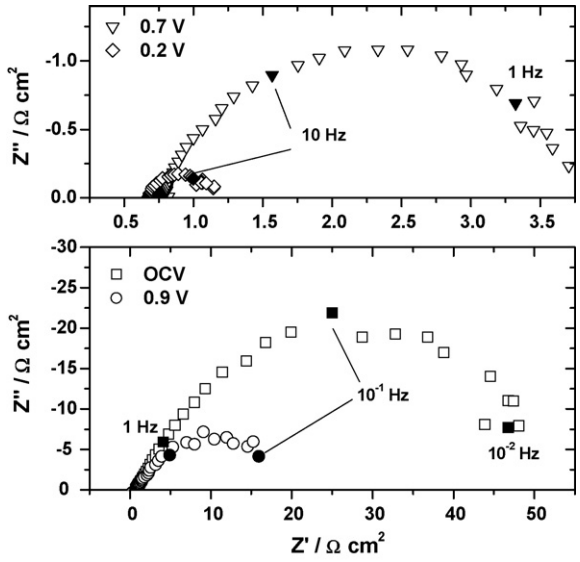

Fig. 5. Impedance spectra of cathode in the third measurement of *I–V* curve in Fig. 2.

model for each electrode has not been established and is under investigation.

3.2. Humidity dependence

Fig. 6 shows *I–V* curves measured at 200 °C under various humidity conditions. Humidified gases with a ratio of *x*% H_2O–(100−*x*)% H_2 and *x*% H_2O–(100−*x*)% O_2 were supplied as fuel and oxidant, respectively. Open circuit voltage was dependent on the humidity due to the change in partial pressure of reactant gases. The performance was enhanced with an increase in humidity up to 30%. In response to this behavior, both *IR* loss and polarization resistance were reduced (Fig. 7). These can be explained by the humidity dependence of electrolyte conductivity [16,18]. Under low humidity conditions, the conductivity decreases accompanied with weight loss due

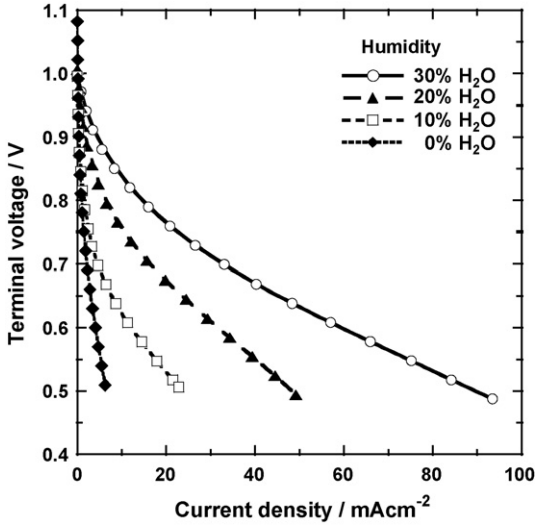

Fig. 6. *I–V* characteristics of a single cell under 0–30% H_2O conditions at 200 °C: (0–30% H_2O/H_2, Pt/C|CsH_2PO_4/SiP_2O_7|Pt/C, 0–30% H_2O/O_2).

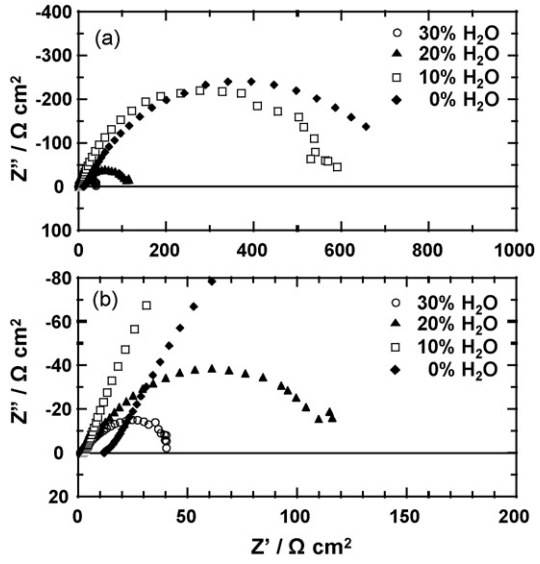

Fig. 7. Impedance spectra of a single cell under 0–30% H_2O conditions at 200 °C, OCV: (a) overall view; (b) magnification figure; (0–30% H_2O/H_2, Pt/C|CsH_2PO_4/SiP_2O_7|Pt/C, 0–30% H_2O/O_2).

to the dehydration and condensation reaction of phosphates. In contrast, it was difficult to discharge stably with supplying fuel and oxidant with 40% H_2O and to maintain the mechanically stable membrane (not shown). Excessive water in fuel and oxidant mixtures should lead to further penetration of molten salt, resulting in the inhabitation of electrode reaction. The anodic and cathodic overpotential under various humidity conditions are shown in Fig. 8(a) and (b), respectively. For both electrodes, a distinct humidity dependence of the overpotential was observed; *i.e.*, the overpotential was reduced with an increase in humidity despite a decrease in partial pressure of reactant gas species. These indicate that the polarization behavior is strongly affected by the difference in electrolyte conductivity under humidified conditions. Additionally the anodic overpotential was considerably lower than the cathodic one regardless of the humidity. This is because the exchange current density of hydrogen oxidation on platinum surface is greater than that of oxygen reduction by a factor of 10^7 under PAFC operating conditions [23]. Thus, the development of excellent electrocatalysts for cathode will be the key factor for the realization of intermediate-temperature fuel cells. The reaction mechanism of hydrogen oxidation over Pt in phosphoric acid can be described in following two elementary steps:

- Tafel step:

$$H_2 \rightarrow 2H(a) \quad (1)$$

- Volmer step:

$$H(a) \rightarrow H^+ + e \quad (2)$$

where H(a) represents atomic hydrogen which is chemisorbed to a metal surface. The Tafel step is generally believed to be the rate-determining step (RDS). Vogel et al. have derived the theoretical equations, correlation between current density and

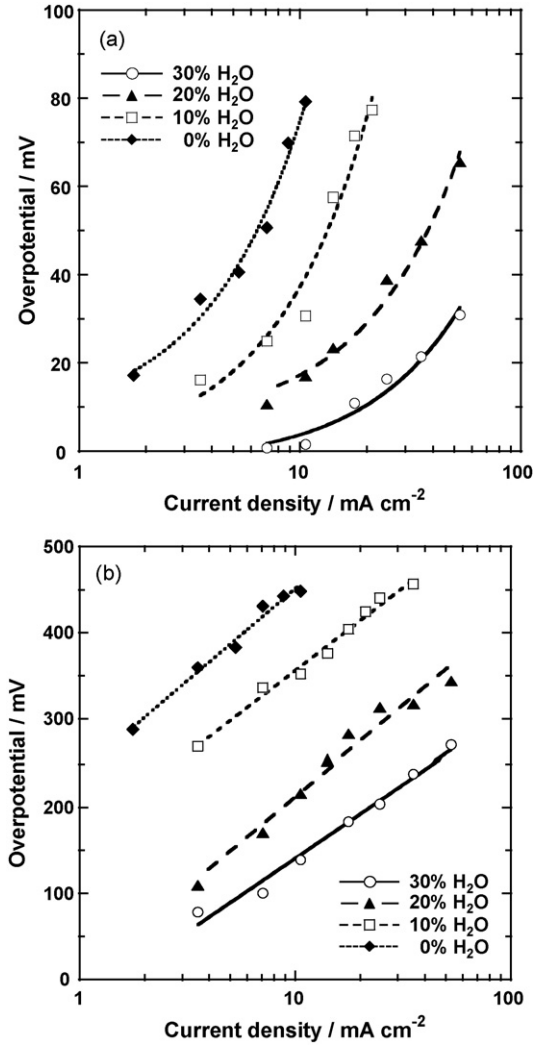

Fig. 8. Electrode overpotential under 0–30% H_2O conditions at 200 °C: (a) anode; (b) cathode.

overpotential, with considering the RDS and the hydrogen concentration gradient in the electrocatalyst layer [24]. In this study, however, it is difficult to apply these equations due to the humidity dependence of electrode polarization. Since the steam-rich fuel is supplied to anode, binary gas diffusion of hydrogen-steam in the catalyst layer has to be also well considered.

In the case of cathode, the overpotential, η, showed a linear dependence against the log of current density. This correlation can be described as follows, which is well known as the Tafel equation:

$$\eta = \frac{2.303RT}{n\alpha F} \log \frac{i}{i_0} \quad (3)$$

where T is the temperature, R is the gas constant, F is the Faraday's constant, n is the number of exchanged electrons, α is the symmetry factor, i and i_0 are current density and exchange current density, respectively [25]. The Tafel slope and exchange current density at cathode were calculated (Table 1). It is noted that the Tafel slope is almost the same within the experimental range of relative humidity (RH), 0–2.0%, at 200 °C. This indi-

Table 1
Kinetics parameters under various humidified atmospheres at 200 °C

Supplied gas	Relative humidity (%)	Tafel slope (mV decade^{-1})	Exchange current density (mA cm^{-2})	αn
70%O_2–30%H_2O	2.0	192	2.05	0.49
80%O_2–20%H_2O	1.3	204	9.34×10^{-1}	0.46
90%O_2–10%H_2O	0.64	193	1.42×10^{-1}	0.49
100%O_2	0	214	7.77×10^{-2}	0.44

cates that there is no change in the reaction mechanism under these conditions. The mechanism of oxygen reduction reaction is discussed in the following section. With an increase in humidity, the exchange current density increased. This phenomenon is different from the case of Pt/H_3PO_4 doped polybenzimidazole (PBI-H_3PO_4) system at 150 °C: the exchange current density was unchanged within the RH range of 1–10% though the range of steam concentration in oxygen was almost the same in this experiment [26]. This can be explained by the difference in the proton-conduction mechanism: the conductivity in PBI-H_3PO_4 system is independent of the water. In the case of CsH_2PO_4/SiP_2O_7-based composite, thus, it was suggested that the adequate amount of steam is required for the fast oxygen reduction reaction.

3.3. Temperature dependence

Fig. 9 shows the *I–V* curves measured in the temperature range of 180–240 °C. In these experiments, the steam concentration in supplying gases was fixed as 30% at every temperature: thus the RH is different depending on the temperature. The *I–V* characteristics were enhanced with increasing temperature up to 220 °C, and the maximum power density of 68 mW cm^{-2} was obtained at 0.42 V (not shown). However, the performance was deteriorated at 240 °C. This can be explained by the deterioration of electrolyte with time due to the dehydration and condensation of phosphates. In response to these reactions, the significant increase in ohmic resistance was observed in impedance spectra (not shown). The corresponding overpotentials at anode and cathode are shown in Fig. 10(a) and (b), respectively. Although the overpotential was reduced with temperature up to 220 °C for both electrodes, the relative humidity in the feed gas significantly affected the electrode kinetic as described above. Thus, the optimum condition has to be well considered at each temperature. It is apparent that performance limitations are dominantly due to the cathodic overpotential even above 200 °C. The cathodic overpotential *vs*. log of current density exhibited a linear dependence at every temperature. Similar single Tafel slope has been reported for Pt/H_3PO_4 with various H_3PO_4 concentration and

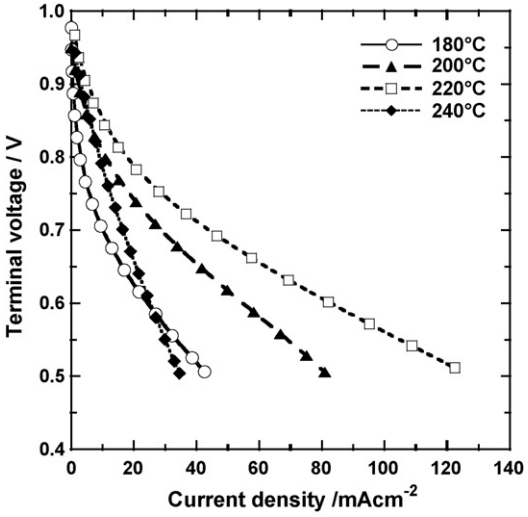

Fig. 9. *I–V* characteristics of a single cell at 180–240 °C under 30% H_2O condition (30% H_2O/H_2, Pt/C|CsH_2PO_4/SiP_2O_7|Pt/C, 30% H_2O/O_2).

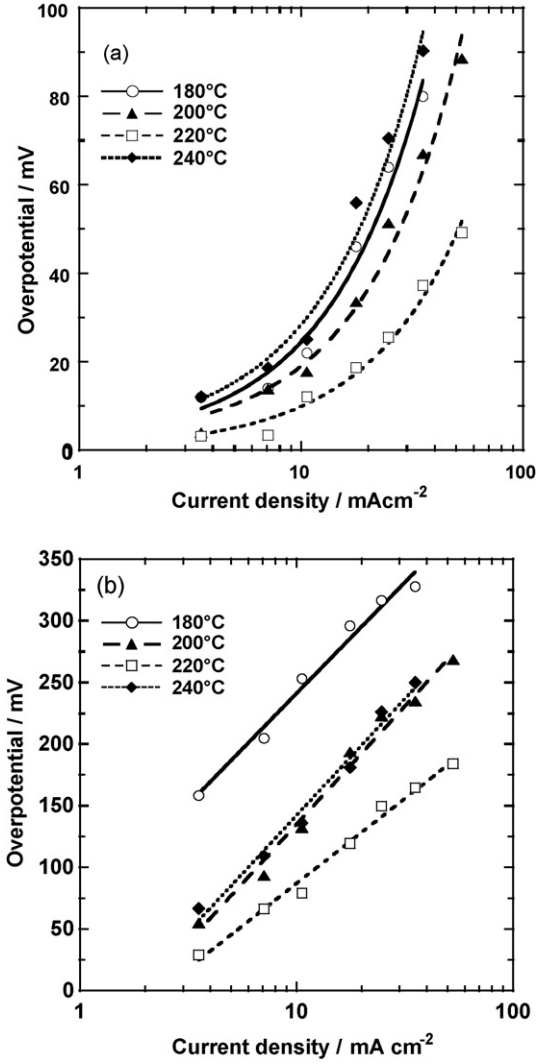

Fig. 10. Electrode overpotential at 180–240 °C under 30% H_2O condition: (a) anode; (b) cathode.

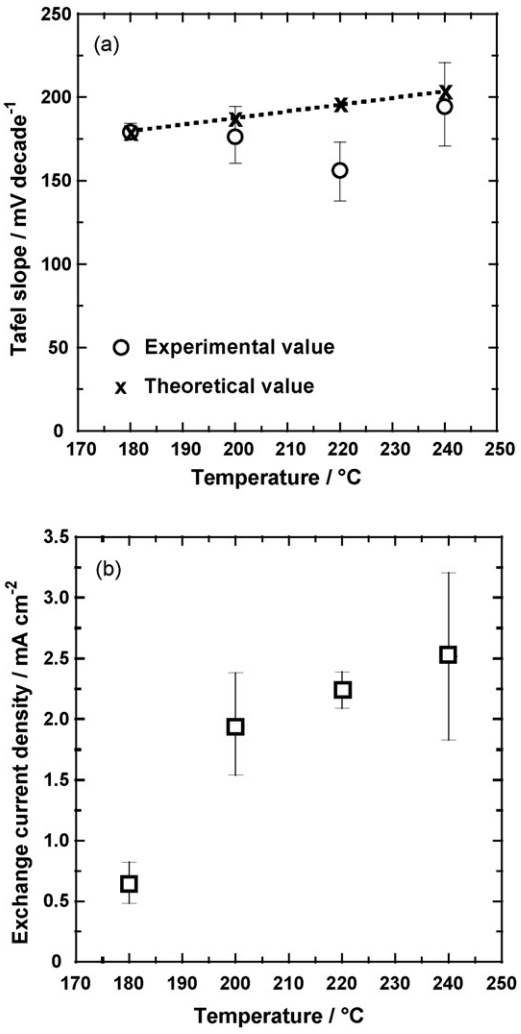

Fig. 11. Kinetics parameters as a function of operating temperature: (a) Tafel slope; (b) exchange current density.

at different temperatures [27–29]. The kinetics parameters were calculated by using the Tafel equation as a function of temperature in Fig. 11. The oxygen reduction reaction can be written as follows [30,31]:

$$O_2 + M \rightarrow M\text{–}O_2 \quad (4)$$

$$O_2 + H^+ + e^- + M \rightarrow M\text{–}O_2H \quad (5)$$

$$M\text{–}O_2H + M \rightarrow M\text{–}OH + M\text{–}O \quad (6)$$

$$M\text{–}O + H^+ + e^- \rightarrow M\text{–}OH \quad (7)$$

$$M\text{–}OH + H^+ + e^- \rightarrow M + H_2O \quad (8)$$

The broken line in Fig. 11(a) is the temperature dependence of Tafel slope that assumed $\alpha = 0.5$. The Tafel slope at each temperature roughly agreed with the value of $2 \times 2.303RT/F$, indicating that the single reaction mechanism is operative in this temperature range. At this stage, it can be expected that the proton transfer is the rate-determining step (Eq. (5)) at intermediate temperature and low RH. In fact, the symmetry factor of α estimated from the experiment was 0.45–0.50. However, the reaction order against the partial pressure of oxygen and proton concentration has not been sufficiently analyzed yet, and the further investigation is required to resolve the reaction mechanism. The exchange current density was continuously enhanced with temperature despite the cell performance deterioration at 240 °C. Therefore, these results also suggest that the water management is very important to avoid the electrolyte deterioration at intermediate temperatures.

4. Conclusions

The polarization behaviors of platinum electrode for both in anode and cathode were investigated with a single cell employing CsH_2PO_4/SiP_2O_7-based composite electrolyte at intermediate temperatures. The spontaneous formation of active TPB was observed during discharge cycles. The preparation method of MEA has to be optimized for oxoacid-based electrolytes. The performance limitation was mainly due to cathodic polarization at every condition. The cathodic overpotential can be expressed as Tafel equation. The exchange current density was enhanced with an increase in relative humidity and temperature, though the Tafel slope was almost independent of these conditions. Thus, these results indicate that the oxygen reduction reaction proceeds based on the same mechanism. The anodic polarization exhibited the similar dependency on humidity and temperature as in the case of cathode. Therefore, the optimization of humidity condition as well as the development of highly active cathode will be the key factors for the realization of intermediate-temperature fuel cells.

Acknowledgments

This work was supported by the Research and Development of Polymer Electrolyte Fuel Cells group of the New Energy and Industrial Technology Development Organization (NEDO) of Japan.

References

[1] N. Wagner, M. Schulze, Electrochim. Acta 48 (2003) 3899.
[2] M. Ciureanu, S.D. Mikhailenko, S. Kaliaguine, Catal. Today 82 (2003) 195.
[3] T. Smolinka, M. Heinen, Y.X. Chen, Z. Jusys, W. Lehnert, R.J. Behm, Electrochim. Acta 50 (2005) 5189.
[4] S.M. Haile, D.A. Boysen, C.R.I. Chisholm, R.B. Merle, Nature 410 (2001) 910.
[5] D.A. Boysen, T. Uda, C.R.I. Chisholm, S.M. Haile, Science 303 (2004) 68.
[6] T. Matsui, S. Takeshita, Y. Iriyama, T. Abe, Z. Ogumi, J. Electrochem. Soc. 152 (2005) A167.
[7] T. Kukino, R. Kikuchi, T. Takeguchi, T. Matsui, K. Eguchi, Solid State Ionics 176 (2005) 1845.
[8] H. Muroyama, T. Matsui, R. Kikuchi, K. Eguchi, J. Electrochem. Soc. 153 (2006) A1077.
[9] J. Otomo, N. Minagawa, C.-J. Wen, K. Eguchi, H. Takahashi, Solid State Ionics 156 (2003) 357.
[10] T. Matsui, S. Takeshita, Y. Iriyama, T. Abe, Z. Ogumi, Solid State Ionics 178 (2007) 859.
[11] M. Nagao, A. Takeuchi, P. Heo, T. Hibino, M. Sano, Electrochem. Solid-State Lett. 9 (2006) A105.
[12] P. Heo, H. Shibata, M. Nagao, T. Hibino, M. Sano, J. Electrochem. Soc. 153 (2006) A897.

[13] H. Shigeoka, J. Otomo, C.J. Wen, M. Ogura, H. Takahashi, J. Electrochem. Soc. 151 (2004) J76.
[14] T. Tezuka, K. Tadanaga, A. Hayashi, M. Tatsumisago, Solid State Ionics 177 (2006) 2463.
[15] A. Matsuda, T. Kikuchi, K. Katagiri, Y. Daiko, H. Muto, M. Sakai, Solid State Ionics 178 (2007) 723.
[16] T. Matsui, T. Kukino, R. Kikuchi, K. Eguchi, Electrochem. Solid-State Lett. 8 (2005) A256.
[17] T. Matsui, T. Kukino, R. Kikuchi, K. Eguchi, J. Electrochem. Soc. 153 (2006) A339.
[18] T. Matsui, T. Kukino, R. Kikuchi, K. Eguchi, Electrochim. Acta 51 (2006) 3719.
[19] H. Fukunaga, M. Ihara, K. Sakaki, K. Yamada, Solid State Ionics 86 (1996) 1179.
[20] H.S. Song, W.H. Kim, S.H. Hyun, J. Moon, J. Kim, H.-W. Lee, J. Power Sources 167 (2007) 258.
[21] J.P. Hoare, in: P. Delahay (Ed.), Advances in Electrochemistry and Electrochemical Engineering, vol. 6, John Wiley & Sons Inc., 1967, p. 201.
[22] Y.-G. Ryu, S.-I. Pyun, C.-S. Kim, D.-R. Shin, Carbon 36 (1998) 293.
[23] M.B. Cutlip, S.C. Yang, P. Stonehart, Electrochim. Acta 36 (1991) 547.
[24] W. Vogel, J. Lundquist, P. Ross, P. Stonehart, Electrochim. Acta 20 (1975) 79.
[25] O.A. Petrii, R.R. Nazmutdinov, M.D. Bronshtein, G.A. Tsirline, Electrochim. Acta 52 (2007) 3493.
[26] Z. Liu, J.S. Wainright, M.H. Litt, R.F. Savinell, Electrochim. Acta 51 (2006) 3914.
[27] D. Chu, Electrochim. Acta 43 (1998) 3711.
[28] K.-L. Hsueh, E.R. Gonzalez, S. Srinivasan, J. Electrochem. Soc. 131 (1984) 823.
[29] J.T. Glass, G.L. Cahen, G.E. Stoner, J. Electrochem. Soc. 136 (1989) 656.
[30] D.S. Gnanamuthu, J.V. Petrocelli, J. Electrochem. Soc. 114 (1967) A1036.
[31] W.M. Vogel, J.M. Baris, Electrochim. Acta 22 (1977) 1259.